Modelling of micro- and nanodomain arrays recorded in ferroelectrics-semiconductors by using atomic force microscopy

A.N. Morozovska
V. Lashkaryov Institute of Semiconductor Physics, NAS of Ukraine
41, prospect Nauky, 03028 Kyiv, Ukraine
E-mail: morozo@i.com.ua

Abstract. The thermodynamical theory of nanodomain tailoring in ferroelectrics-semiconductors allowing for semiconducting properties, screening and size effects is presented. The obtained analytical results prove that domains appearance is similar to the first order phase transition and completely agree with experimentally observed threshold nanodomains recording in $Pb(Zr,Ti)O_3$ and $LiTaO_3$ thin films. The realistic dependence of equilibrium nanodomain radius over applied voltage in $BaTiO_3$, $LiNbO_3$ ferroelectric-semiconductors, $LiTaO_3$ and $Pb(Zr,Ti)O_3$ thin films have been calculated. These results will help researchers both to achieve the reliable understanding of physical process taking place during nanoscale polarization reversal in the ferroelectric-semiconducting media and to determine the necessary conditions in order to record stable nanodomains with optimum lateral sizes and configuration to increase recording density and create various profiled microstructures.

Keywords: ferroelectric nanodomains, screening effects, atomic force microscopy, information recording.

Manuscript received 13.12.05; accepted for publication 29.03.06.

1. Introduction

Ferroelectric micro- and nanodomains (submicron spatial regions with reversed spontaneous polarization) can be created by inhomogeneous electric and/or elastic fields with definite polarity in many ferroelectrics-semiconductors and photorefractive ferroelectrics [1-3]. Recently, one and two dimensional arrays of stable nanodomains have been tailored in $LiNbO_3$ [4, 5], $LiTaO_3$ [6], $Pb(Zr,Ti)O_3$ [7-10], $BaTiO_3$ [11] and $RbTiOPO_4$ [12] ferroelectric materials using the electric fields caused by an atomic force microscope (AFM). The experimental and theoretical study of submicron- and nanodomain tailoring in a ferroelectric media attract the broad interest owing to its possible applications in many fields of nanophysics and nanotechnology, namely: various nanostructures assembling for modern electronic and electromechanical devices [13], nonlinear and fine optical elements [4, 12], high density memory elements based on new physical principles [6, 7, 14]. From the fundamental viewpoint, formation of artificial nanodomains is a promising field for the direct observation of size, surface and interface effects of the domain structure and switching kinetics [9, 10].

However, in order to achieve these purposes it is necessary to develop an adequate physical model of the spontaneous polarization local reversal. Such models can help not only to optimize the problem of nanodomain writing with a high density and stability, but also to achieve a satisfactory understanding of complex physical processes taking place during the nanoscale polarization reversal.

However, existing phenomenological models give an incomplete picture of the nanodomain formation owing to the following reasons.

- Landauer [15] considered the domains nucleation during the polarization reversal in the *homogeneous* electric field. In this model, surface bond charges are compensated by the free charges on the flat metallic electrodes.

- Molotskii [16] evolved the model of domain formation inside the perfect ferroelectric-dielectric with free surface under the *inhomogeneous* electric field of AFM tip. However, he considered the depolarization field in the framework of the Landauer model as if the perfect external screening expected, although a nanosized AFM tip apex could be hardly treated as the plain electrode.

- In our recent papers [3, 17-19], we have tried to overcome the aforementioned discrepancies taking into consideration screening layers of immovable surface charges and semiconductor properties revealed by the most of ferroelectrics (see [2, 20-22]). In the most of

experiments [4-12], the screening layer recharging is quite possible due to the field emission caused by the positively charged AFM tip [18, 19].

• Nanodomain tailoring in the thin ferroelectric film seems more useful for applications than domain recording in a relatively thick layer, allowing for possible miniaturization of functional elements. As far as we know, a theoretical description of nanodomain recording in thin ferroelectric films is in the initial stage; in particular, semiconductor properties of films are neglected (see *e.g.* [23-25]).

2. Theoretical consideration of domain origin in ferroelectrics-semiconductors

Let us consider a solid ferroelectric with spontaneous polarization $\mathbf{P}_S$, dielectric permittivity ε_i, electrical induction $\mathbf{D} = \varepsilon_i \cdot \mathbf{E} + 4\pi \mathbf{P}_S$, electric field $\mathbf{E} = -\nabla\varphi(\mathbf{r})$ ($\varphi(\mathbf{r})$ is the electrostatic potential). We choose the spontaneous polarization $+P_S$ inside and $-P_S$ outside the domain (see Fig. 1). The AFM tip electric field is calculated in the spherical model, in which the charged sphere with radius R_0 substitutes the real tip. The validity of such approach for dielectric sample and other models are discussed in [26]. The voltage U is applied between the tip and bottom electrode.

Surface charges with $\sigma_S = -P_S$ were captured on the sluggish trap levels before the domain formation

[27]. Usually $\Delta R < 1$ nm [4-12], thus, field emission is quite possible at applied voltages $U \geq U_m$. Keeping in mind the approach proposed in [28] for current-voltage characteristics of ferroelectric tunnel junctions as well as interface screening model evolved in [29], we assume that the switching current $J_e \sim \exp(-U_m/U)$. At applied voltages $U \geq U_m$, the amount of emitted carriers are quite enough to completely screen the reversed polarization of the domain butt-end [24, 30], *i.e.*, $\sigma_S \rightarrow +P_S$ at $U > U_m$. Thus, interpolation for the equilibrium surface charge density σ_S has the form:

$$\sigma_S = \begin{cases} -P_S + 2P_S \exp(-U_m/U), & \sqrt{x^2 + y^2} < d \\ -P_S, & \sqrt{x^2 + y^2} > d \end{cases} \quad (1)$$

In a general case, the activation voltage U_m in some complex manner depends on the distance ΔR, sample thickness h, *etc*. For the thin film, we assume that $U_m \cong E_m h$, where E_m is the so-called activation field [1].

Another important experimental fact should be taken into consideration for the correct theoretical description of nanodomain tailoring using AFM tip. Namely, it seems quite probable that on the polar oxide surface thin water layers are quite possible [8, 25, 31]. Moreover, if AFM tip is wettable, its apex with curvature 25-50 nm can be completely covered with
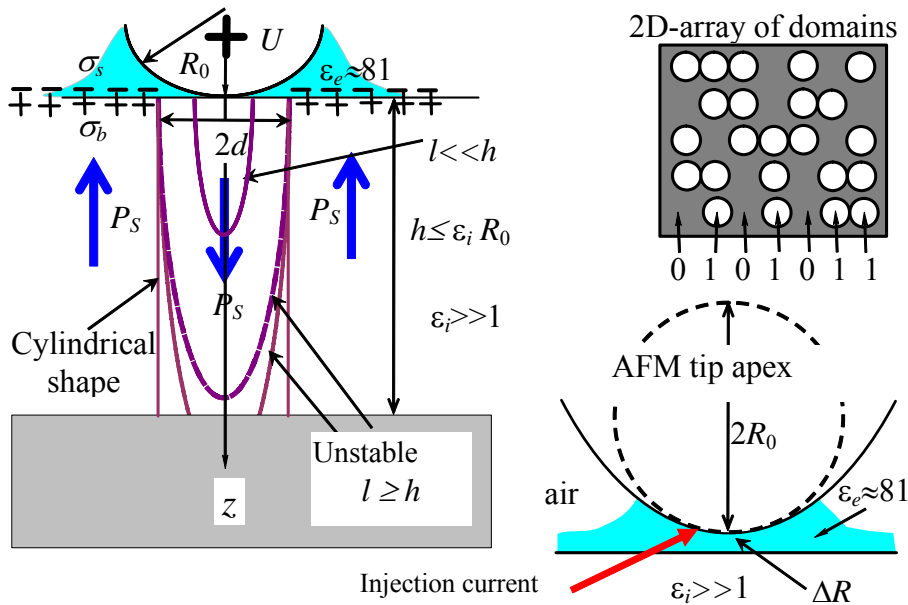
Fig. 1. Nanodomain growth through the thin ferroelectric film. U is the applied voltage, ΔR is the distance between the tip apex and sample surface, R_0 is the tip radius of curvature, d is the domain radius, l is the domain length, h is the film thickness, P_S is the spontaneous polarization, σ_S is the density of surface charges captured on the sluggish trap levels, σ_b is the density of bound charges related to P_S discontinuity.

water [32]. Hereinafter, we regard that this region has the effective dielectric permittivity ε_e.

Electric field screening is realized by free charges with the bulk density $\rho_f(\mathbf{r}) \approx -\varepsilon_i(\mathbf{r})/4\pi R_d^2$ (R_d is the Debye screening radius). The electrostatic potential spatial distribution should be determined from the Maxwell equation $\varepsilon_i \Delta\varphi(\mathbf{r}) = -4\pi\rho_f(\mathbf{r})$ supplemented with the interfacial conditions $D_{n\,\text{int}} = D_{n\,\text{ext}}$ on the domain surface Σ, $D_{n\,\text{int}} - D_{n\,\text{ext}} = 4\pi\sigma_S$ on the free surface $z = 0$. Thus, we obtain the following boundary problem:

$$\Delta\varphi_0(\mathbf{r}) = 0, \qquad z \leq 0,$$

$$\varphi_0\big|_{\mathbf{r}\in\text{tip}} = U, \qquad \varphi_0\,(z=0) = \varphi\,(z=0),$$

$$\left(\varepsilon_e \frac{\partial\varphi_0}{\partial z} - \varepsilon_i \frac{\partial\varphi}{\partial z}\right)\Bigg|_{z=0} = \begin{cases} 4\pi(\sigma_S - P_S), & \sqrt{x^2+y^2} < d, \\ 0, & \sqrt{x^2+y^2} > d, \end{cases}$$

$$\Delta\varphi(\mathbf{r}) - \frac{\varphi(\mathbf{r})}{R_d^2} = 0, \qquad z \geq 0,$$

$$\varepsilon_i\left(\frac{\partial\varphi_{\text{int}}}{\partial n} - \frac{\partial\varphi_{\text{ext}}}{\partial n}\right)\Bigg|_\Sigma = 8\pi(\mathbf{P}_S\mathbf{n})\big|_\Sigma, \quad \varphi(z=h) = 0.$$

(2)

In order to apply all the following results to the anisotropic semiconductor, one can make the substitution $z \to z\sqrt{\varepsilon_a/\varepsilon_c}$, $l \to l\sqrt{\varepsilon_a/\varepsilon_c}$, $\varepsilon_i \to \sqrt{\varepsilon_c\varepsilon_a}$, $R_d^2 = \dfrac{\varepsilon_a\,k_B\,T}{4\pi\,e^2\,n_d}$. Here ε_a and ε_c are anisotropic dielectric permittivity values perpendicular and parallel to the polar axis z.

Our calculations [18, 19] have shown that in the thick films with the thickness $h \gg R_d$ (when $\exp(-h/R_d) \ll 1$) the equilibrium domain length l almost always is much greater than its radius d, *i.e.*, usually semi-ellipsoidal domains are spike-like. In contrast to the thick films, equilibrium domains usually grow through the thin film with the thickness

$h \leq \sqrt{\varepsilon_c\varepsilon_a}\cdot R_0$ and reach the bottom electrode, *i.e.*, such domains have rather a cylindrical shape than the semi-ellipsoidal one (see *e.g.* [9]).

Electrostatic energy $\Delta\Phi_{\text{el}}(d,l) =_U(d,l) + \Phi_D(d,l)$ of the domain recorded in the anisotropic ferroelectric-semiconducting sample is derived in [18, 19]. The energy $\Delta\Phi_{\text{el}}(d,l)$ and domain wall surface energy $\Phi_C(d,l)$ contribute into the free energy $\Phi(d,l)$:

$$\Phi(d,\,l) = \Phi_C(d,\,l) + \Phi_U(d,\,l) + \Phi_D(d,\,l). \tag{3}$$

Below, we consider each term in (3), under the condition $\Delta R \ll R_0$ typical for the most of experiments [4-12].

a) The domain wall surface energy $\Phi_C(d,l)$ has the form:

$$\Phi_C(d,\,l) = \begin{cases} \dfrac{\pi^2\psi_S\,d\,l}{2} & \text{prolate semi-ellipsoidal} \\ & \text{domain with } d \ll l, \\ 2\pi d\,\psi_S\,h & \text{cylindrical domain.} \end{cases} \tag{4}$$

We regard domain walls as infinitely thin, with the homogeneous surface energy density ψ_S. This assumption used by many authors [15, 16, 25, 33] was confirmed both by the modern first principle calculations (*e.g.* [34-36]) and recent experimental data (*e.g.* [37-39]), which revealed that the domain wall thickness in perovskite ferroelectrics is about several lattice parameters. Depending on the sample preparation and experiment conditions, the measured energy ψ_S differs by several unities to several hundreds of times (*e.g.* 0.1-10 mJ/m² for BaTiO₃ [1], 9-200 mJ/m² for LiTaO₃ [39, 40] and references therein). Taking into account the aforementioned facts, we regard the effective surface energy ψ_S as a fitting parameter that can vary within the range 10^{-1} to 10^2 mJ/m².

b) The energy $\Phi_U(d,l)$ is caused by interaction between the tip electric field and reversed polarization inside the domain. Pade approximation for the interaction energy $\Phi_U(d,l)$ acquires the following form [18, 19]:

$$\Phi_U(d) =$$

$$= \begin{cases} \dfrac{\sqrt{\varepsilon_a\varepsilon_c} + \varepsilon_e}{\sqrt{\varepsilon_a\varepsilon_c} - \varepsilon_e}\ln\left(\dfrac{\sqrt{\varepsilon_a\varepsilon_c} + \varepsilon_e}{2\varepsilon_e}\right) \times \dfrac{4\pi\varepsilon_e(\sigma_S - P_S)\cdot UR_0 R_d\left(\sqrt{R_0^2+d^2} - R_0\right)}{\left(\sqrt{\varepsilon_a\varepsilon_c} + \varepsilon_e\right)R_d + 2\sqrt{\varepsilon_a\varepsilon_c}\sqrt{R_0^2+d^2}}, & \begin{array}{l} d \ll l \\ h \gg R_d \end{array} \\[6mm] \dfrac{\sqrt{\varepsilon_a\varepsilon_c} + \varepsilon_e}{\sqrt{\varepsilon_a\varepsilon_c} - \varepsilon_e}\ln\left(\dfrac{\sqrt{\varepsilon_a\varepsilon_c} + \varepsilon_e}{2\varepsilon_e}\right) \times \dfrac{4\pi\varepsilon_e(\sigma_S - P_S)\cdot UR_0\cdot hR_d\left(\sqrt{R_0^2+d^2} - R_0\right)}{\left(\sqrt{\varepsilon_a\varepsilon_c} + \varepsilon_e\right)hR_d + \sqrt{\varepsilon_a\varepsilon_c}(R_d + 2h)\sqrt{R_0^2+d^2}}, & h \leq \sqrt{\varepsilon_c\varepsilon_a}R_0. \end{cases} \tag{5}$$

At $R_d \to \infty$, $h \to \infty$ and $\sigma_S \to -P_S$, $\varepsilon_e = 1$ the energy (5) coincides with the one calculated in [16].

c) The depolarization field energy $\Phi_D(d,l) = \Phi_{DL}(d,l) + \Phi_{DS}(d)$ is caused by local polarization reversal. The Landauer energy $\Phi_{DL}(d,l)$ is absent for the cylindrical domain that reached the bottom electrode. Pade approximation for the Landauer energy of the prolate semi-ellipsoidal domain acquires the form [18, 19]:

$$\Phi_{DL}(d,l) \approx$$

$$\approx \begin{cases} \dfrac{16\pi^2 P_S^2}{\sqrt{\varepsilon_a \varepsilon_c}} \dfrac{d^4 R_d \left(\ln\left(2\sqrt{\varepsilon_a/\varepsilon_c} \cdot l/d\right)-1\right)}{3\sqrt{\varepsilon_a/\varepsilon_c}\, l\, R_d + 4d^2\left(\ln\left(2\sqrt{\varepsilon_a/\varepsilon_c} \cdot l/d\right)-1\right)}, \\[2mm] \qquad\qquad\qquad\qquad\qquad d \ll l \\ \qquad\qquad\qquad\qquad\qquad h \gg R_d \\[4mm] 0, \qquad\qquad\qquad\qquad h \le \sqrt{\varepsilon_c \varepsilon_a} \cdot R_0. \end{cases}$$

$$(6)$$

The energy (6) coincides with that calculated in [16] at $R_d \to \infty$. The domain butt energy $\Phi_{DS}(d)$ has the form [19]:

$$\Phi_{DS}(d) \approx$$

$$\approx \begin{cases} \dfrac{\pi^2 (\sigma_S - P_S)^2 d^3 R_d}{\sqrt{\varepsilon_a \varepsilon_c}\, d + \left(\sqrt{\varepsilon_a \varepsilon_c} + \varepsilon_e\right) 3\pi R_d/16}, \\[2mm] \qquad\qquad\qquad d \overset{>}{\sim} R_0/2, \quad h \gg R_d, \\[4mm] \dfrac{\pi^2 (\sigma_S - P_S)^2 d^3 h R_d}{h\left(\sqrt{\varepsilon_a \varepsilon_c}\, d + \left(\sqrt{\varepsilon_a \varepsilon_c} + \varepsilon_e\right) 3\pi R_d/16\right) + \sqrt{\varepsilon_a \varepsilon_c}\, R_d d/2}, \\[2mm] \qquad\qquad\qquad h \le \sqrt{\varepsilon_c \varepsilon_a}\, R_0. \end{cases}$$

$$(7)$$

It should be noted that the similar problem of domain intergrowth through the thin ferroelectric-dielectric film was considered by Molotskii [25]. However, the depolarization field energy dependence on the film thickness and domain radius was chosen as d^2h under the condition $h \gg d$. As it follows from our energy (7), the dependence d^2h can be expected in the opposite case $h \ll d$ [19].

The free energy (3) dependence on the domain radius for various values of the applied voltage is represented in Fig. 2. It is clear from Fig. 2 that the free energy has no minimum at small voltages. With the voltage increase, the absolute minimum $\Phi_{\min} < 0$ appears at a critical value of the domain radius $d_{\min}$. Under the further voltage increase, the radius of the stable domain increases.

It is clear from Fig. 2 that there is a potential barrier between $d = 0$ (domain is absent) and $d \ne 0$ (domain exists). The relative height of this barrier decreases with
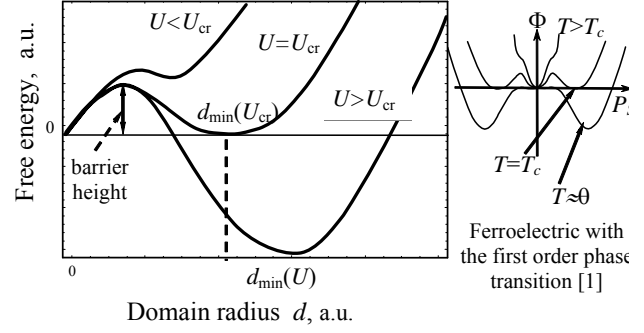
Fig. 2. Schematic free energy dependence on the domain radius d for the prolate semi-ellipsoidal or cylindrical inter-grown domains at different applied voltage values U (left plot). Compare it with a typical free energy dependence on polarization P_S at different temperatures T for ferroelectric with the first order phase transition (right plot).

applied voltage increase. That is why, the domain radius does not decrease continuously with voltage decrease: the stable domain appears with a non-zero radius $d = d_{\min}$ at $U \ge U_{\mathrm{cr}}$, *i.e.*, when homogeneous polarization distribution becomes unstable. Such "threshold" domain formation is similar to the well-known first order phase transition. At lower voltages $U < U_{\mathrm{cr}}$, domain formation becomes energetically impossible. This result seems to be quite reasonable, because the most of stable ferroelectric nanodomains were recorded only above some critical voltage $U_{\mathrm{cr}} \sim (3\ldots6)$ V (see *e.g.* [6-8]).

From the condition $\Phi_{\min}(d_{\min}, U) = 0$, we derived the following expressions for U_{cr} and $d_{\min}(U_{\mathrm{cr}})$ determination valid for nanodomain recording in the thin film with $h \ll R_d$, $h \le \sqrt{\varepsilon_c \varepsilon_a} R_0$:

$$U_{\mathrm{cr}}(h) \approx \sqrt{\frac{32\psi_S}{3}} \frac{\sqrt{\varepsilon_a \varepsilon_c}\, R_0 + \left(\sqrt{\varepsilon_a \varepsilon_c} + \varepsilon_e\right)h}{\sqrt{\left(\sqrt{\varepsilon_a \varepsilon_c} + \varepsilon_e\right)h}} \times$$

$$\times \left(\varepsilon_e \frac{\sqrt{\varepsilon_a \varepsilon_c} + \varepsilon_e}{\sqrt{\varepsilon_a \varepsilon_c} + \varepsilon_e} \ln\left(\frac{\sqrt{\varepsilon_a \varepsilon_c} + \varepsilon_e}{2\varepsilon_e}\right)\right)^{-1}, \qquad (8)$$

$$d_{\min}(U_{\mathrm{cr}}) \approx \sqrt{\frac{3\psi_S\left(\sqrt{\varepsilon_a \varepsilon_c} + \varepsilon_e\right)}{8\left(\sigma_S(U_{\mathrm{cr}}) - P_S\right)^2}}\, h. \qquad (9)$$

It is clear from (9) that in order to record domains with a minimum radius, it is necessary to choose the ferroelectric medium with high spontaneous polarization P_S, small domain wall energy ψ_S and permittivity $\sqrt{\varepsilon_a \varepsilon_c}$, but not very small Debye screening radius (namely it should satisfy the conditions

$R_d \gg h$, $R_d \gg R_0$). Also, it seems urgent to decrease the film thickness h until ferroelectric phase exists [1, 41, 42], but keeping in mind that $(\sigma_S(U_{cr}) - P_S) \sim 2P_S(\exp(-U_m/U_{cr})) - 1$ in accordance with (1) and $U_m \cong E_m h$, the film thickness h should not be extremely small in order to prevent sharp increase of $d_{min}(U_{cr})$ (see denominator in (9)). Taking into account that the threshold field E_m, ψ_S, and R_d could not be directly calculated within the framework of our model, they should be determined as fitting parameters from the experimental dependence $d(U)$. When material parameters E_m, ψ_S, R_d are known and regarded almost independent on the film thickness h, as well as the possible thickness dependence $\varepsilon_{a,c}(h)$ is determined [41], an optimum h value can be calculated numerically from the condition $d_{min}(U_{cr}(h)) = \min$. For the thickness-independent permittivity $\varepsilon_{a,c}$, we derived the approximation:

$$h_{opt} \approx \frac{(32\psi_S/3)^{1/3}}{\sqrt{\varepsilon_a \varepsilon_c} + \varepsilon_e} \left(\frac{\sqrt{\varepsilon_a \varepsilon_c}\left(\sqrt{\varepsilon_a \varepsilon_c} - \varepsilon_e\right)}{\varepsilon_e \ln\left(\sqrt{\varepsilon_a \varepsilon_c} + \varepsilon_e/2\varepsilon_e\right)} \frac{2R_0}{E_m} \right)^{2/3} .$$

(10)

Allowing for the fact that it is much more difficult to change the material parameters E_m, ψ_S, and R_d than the film thickness h, the proposed procedure for the optimum thickness determination seems necessary.

For the majority of experiments [4-7], recorded nanodomains remain unchangeable for many days and weeks. This fact proves their stability and is extremely useful for many applications. It has the following explanation within the framework of the proposed model. When the applied voltage U is turned off, the external field disappears in proportion to U, and the domain depolarization field $E_D = -\nabla \varphi_D \sim (\sigma_S - P_S)$ vanishes due to the surface traps sluggish recharging (*i.e.*, when $\sigma_S \to P_S$). The remained positive surface energy $\Phi_C(d) \sim \psi_S d h$ tends to reverse the domain. In order to move, the domain wall has to overcome the pinning caused by defects, but the tension field $E_W \cong \psi_S/P_S d \sim 100$ kV/cm appeared too small in comparison with the thermodynamic coercive field $E_C \cong 4\pi P_S/\sqrt{\varepsilon_a \varepsilon_c} \sim (250...2700)$ kV/cm regarded necessary for the domain repolarization [8]. Thus, the domain wall pinning does provide the recorded domains stability; surely it also determines the domain growth kinetics [7, 10].

Let us discuss the peculiarities of possible inter-influence between domains during their recording. Neighbour nanodomains can interact via their depolarization fields. If the time interval t between the neighbour domains recording is sufficient for complete recharging the surface traps, depolarization field vanishes and domains inter-influence is absent. Thus, during such process it is possible to obtain independent stable nanodomains with the minimum radius d_{min} at $U \approx U_{cr}$ (see (8) and (9)).

3. Modelling of stable ferroelectric domains

3.1. Screening and size effects on the nanodomains recording in BaTiO$_3$

It should be noted that Eng *et al.* [11] recorded nanodomains with the radius about 30 nm in BaTiO$_3$ crystals at the applied voltage 80 V. The dependence of the equilibrium domain radius d over the applied voltage U is shown in Fig. 3 for various Debye screening radii R_d.

We would like to underline that Debye screening not only decreases depolarization field inside the domain but also shields the AFM tip electric field inside the sample. As a result, the Debye screening radius decrease leads to the decrease of the equilibrium domain radius (compare the lowest curves with the dashed ones). The critical voltage U_{cr} is almost independent over R_d value at small radii of curvature $R_0 \ll R_d$ and distance $\Delta R \ll R_d/\sqrt{\varepsilon_a \varepsilon_c}$, *e.g.* $U_{cr} \approx 2.5$ V corresponds to $R_d \geq 250$ nm (see (8)).
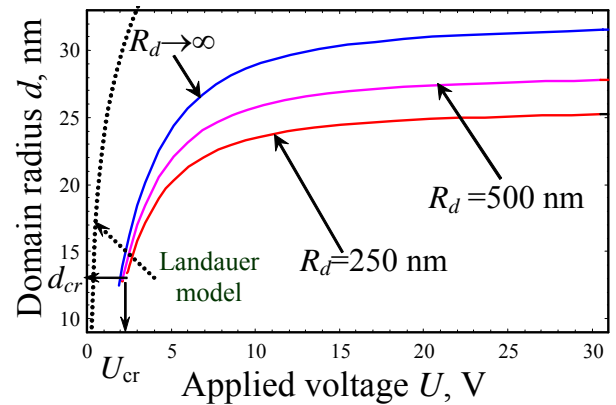
Fig. 3. Equilibrium domain radius d dependence on the applied voltage U for various Debye screening radii R_d (solid curves). Dashed curves represent calculations without domain butt depolarization energy and screening effects (Landauer model [15]). We assume that $\varepsilon_e = 81$, $\Delta R \leq 1$ nm, $R_0 = 25$ nm, $U_m = 1.25$ V and $h \gg R_d$. Other parameters are typical for BaTiO$_3$ [17]: $P_S \approx 26$ µC/cm^2, $\psi_S \approx 8$ mJ/m^2 [36], $\varepsilon_a = 2000$, $\varepsilon_c = 120$.

In a general case, carriers emission leads to the essential decrease of domain sizes at high voltages, namely, the domain growth stops at $U >> U_m$ (see saturated curves for $U > 20\,\text{V}$). Indeed, $\sigma_S \to P_S$ at $U_m \to 0$, and so emitted carriers fully compensate not only the depolarization field caused by the domain butt polarization, but they simultaneously screen the charged tip electric field, which is the reason of domain formation (see (5) and (7)).

Note that the domain butt depolarization field energy (7) essentially decreases the domain sizes even at low voltages [17]. It does not appear in the system considered in [16] due to the complete screening of surface bond charges by the free charge inside the upper electrode (see dotted curves).

In the following section, we'll show that our free energy (3) can be unambiguously reconstructed using experimental dependence $d(U)$, *i.e.*, how the parameters ψ_S, R_d and U_m can be determined. The procedure is rather simple. First, the dependence $d(U)$ should be calculated from (3) and compared with equilibrium domain sizes recorded at definite h, R_0 and ΔR values. The values ε_a, ε_c, ε_e and P_S are regarded known or measured independently for the chosen pair film-substrate. The values ψ_S, R_d and U_m should be determined as fitting parameters from the dependence $d(U)$.

3.2. Submicrodomain recording in LiNbO₃

Let us apply our theoretical results to domain formation in LiNbO₃ single crystals using high-voltage AFM. In experiments [4, 5], the AFM tip radius was $R_0 = 50\,\text{nm}$, distance $\Delta R < 1\,\text{nm}$, maximum applied voltage pulse value $U_{\max} = 4\,\text{kV}$ with duration up to 5 min, sample thickness $h \sim 1\,\text{mm}$. For LiNbO₃ at room temperature, $\varepsilon_a = 84$, $\varepsilon_c = 30$, $P_S \approx 50\,\mu\text{C/cm}^2$, $\psi_S \approx (5...50)\,\text{mJ/m}^2$ (see e.g. [40]). The comparison of experimental results and our calculations is presented in the Fig. 4. The fitting value of the Debye screening radius $R_d > 100\,\mu\text{m}$ is in a reasonable agreement with estimations $R_d \sim (10^4...10^6)\,\text{nm}$ valid for the broad gap ferroelectrics-semiconductors with unavoidable growth defects.

3.3. Nanodomain recording in Pb(Zr,Ti)O₃ and LiTaO₃ thin films

Recently, nanodomain arrays were recorded in Pb(Zr,Ti)O₃ thin films using AFM. In the experiment [7], the AFM tip radius $R_0 = (20...50)\,\text{nm}$, the distance $\Delta R \le 0.3\,\text{nm}$ was difficult to control due to the surface roughness close to $0.2...0.3\,\text{nm}$, applied voltage pulse values varied in the range $U = (4...12)\,\text{V}$ with the duration about 0.1 s. The comparison of experimental results and our calculations is presented in Fig. 5.
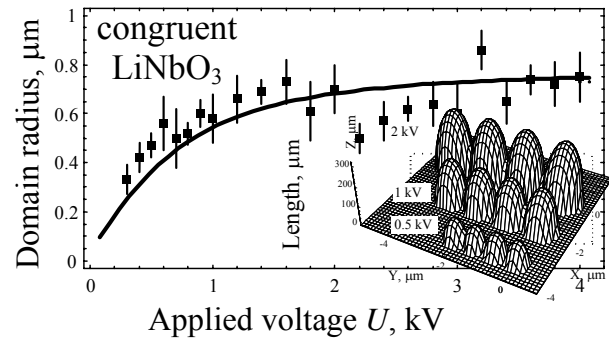

Fig. 4. Equilibrium domain radius and length *vs* the applied voltage U in LiNbO₃. Squares with error bars are experimental data from [4] for the domain radius d, the domain length was estimated as 150 to 250 μm [5], $R_0 = 50$ nm, $\Delta R < < 1$ nm. The solid curve is our fitting at $R_d \ge 100$ μm, $\psi_S \approx \approx 5\,\text{mJ/m}^2$ [40], $U_m = 0.15$ kV, $P_S \approx 50\,\mu\text{C/cm}^2$, $\varepsilon_a = 85$, $\varepsilon_c = = 30$, $\varepsilon_e = 81$. Inset: 3D view of nanodomains arrays recorded in congruent LiNbO₃ sample at variuos voltages U.

Reconstruction of the free energy dependence on the domain radius is performed for several values of the applied voltage U.

The spontaneous polarization P_S and dielectric permittivity components $\varepsilon_{a,c}$ were calculated using coefficients [43] for the bulk PbZr₀.₂Ti₀.₈O₃. It appeared that the value $P_S \approx 70\,\mu\text{C/cm}^2$ coincides with that extracted from the *a/c* ratio measured in the same thin films [37]. The fitting value of the surface energy $\psi_S \approx 140\,\text{mJ/m}^2$ is of the same order as the PbTiO₃ domain wall energy $(100...200)\,\text{mJ/m}^2$ calculated by [34, 35] from the first principles. Thus, our fitting makes it possible to reconstruct the surface free energy value in Pb(Zr,Ti)O₃ thin film.

It is clear from Fig. 5 that the free energy has no minimum at the small voltages $U \le 4\,\text{V}$. With the voltage increase above $U \le 6\,\text{V}$, the absolute minimum $\Phi_{\min}(d) < 0$ appears at the definite value of the domain radius $d \approx 25\,\text{nm}$. With the further voltage increase, the equilibrium domain radius rapidly increases and the stable domain appears (see curves for $U \ge 8\,\text{V}$).

There is a potential barrier between $d = 0$ (domain is absent) and $d \ne 0$ (domain exists). The relative height of this barrier sharply increases with the applied voltage decrease (compare curves for $U = 6\,\text{V}$ and $U = 15\,\text{V}$). That is why, the domain radius does not decrease continuously with the voltage decrease: the domain appears with the non-zero radius $d_{\min} = (U_{\text{cr}})$ at $U > U_{\text{cr}}$. It is seen from the figure that the critical voltage $U_{\text{cr}} \approx 5.7\,\text{V}$, which is in a good agreement with the value reported by Paruch *et al.* [7].
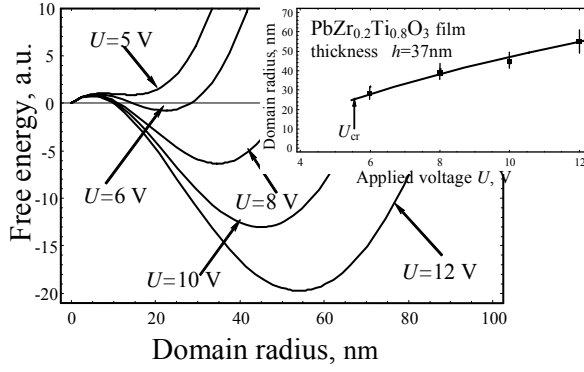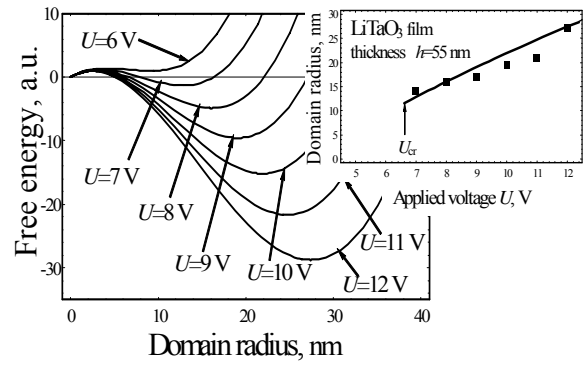
Fig. 5. Free energy dependence on the nanodomain radius and applied voltage (basic plot) was reconstructed from the dependence $d(U)$ (inset). Squares with error bars are experimental data from [7] for nanodomain radius recorded in the $PbZr_{0.2}Ti_{0.8}O_3$ thin film on $SrTiO_3$ substrate with thickness $h = 37$ nm, $\varepsilon_a = 143$, $\varepsilon_c = 86$, $\varepsilon_e = 81$, $P_S \approx 70$ μC/cm^2 [43] and $R_0 = (20...50)$ nm, $\Delta R \leq 0.3$ nm. Solid line is our fitting obtained at $\psi_S \approx 140$ mJ/m^2, $R_d = 1$ μm, $R_0 = 35$ nm, activation voltage $U_m \approx 1.5$ V, $\Delta R \leq 0.5$ nm.

Fig. 6. Free energy dependence on the nanodomain radius (basic plot) reconstructed from the dependence $d(U)$ (inset). Squares are experimental data from [6] for the nanodomain radius recorded in the thin $LiTaO_3$ film with the thickness $h = 55$ nm, $R_0 = 25$ nm. Solid line is our fitting calculated at: $P_S \approx 55$ μC/cm^2, $\varepsilon_a = 53$, $\varepsilon_c = 45$ [40], $\varepsilon_e = 81$, $\psi_S \approx 220$ mJ/m^2, $R_d = 100$ μm, $\Delta R \leq 1$ nm, $U_m \approx 6.5$ V.

The optimization procedure based on (8)-(10) proves that it is possible to record stable domains with $d_{min} \approx 17$ nm at $U_{cr} \approx (6...8)$ V in the films with the thickness $h_{opt} \approx (70...130)$ nm. Thus, information recording with the density 86 Gbit/cm^2 is accessible in the thin PZT films (compare with the density 4 to 28 Gbit/cm^2 reported in [7, 10]).

Note that the activation field fitting value $E_m \approx U_m / h = 405$ kV/cm is in a surprisingly good agreement with the quasi-static coercive field values $E_c \sim (40...400)$ kV/cm typical for thin PZT films (see *e.g.* [20] and refs therein).

Let us apply our theoretical results (3) to (10) to the nanodomain recording in thin congruent $LiTaO_3$ films using high-voltage AFM. Fujimoto *et al.* [6] used the AFM tip with the radius $R_0 = 25$ nm, the maximum applied voltage pulse value was $U_{max} = 11$ V with duration up to 10^{-4} s, and $LiTaO_3$ thin films had the thickness $h = (55...83)$ nm. The comparison of experimental results and our calculations is represented in Fig. 6.

The $LiTaO_3$ domain wall surface energy density ψ_S can vary within the range $(60...400)$ mJ/m^2 (see [40] and refs therein). The spontaneous polarization value $P_S \approx 55$ μC/cm^2 was obtained in the same $LiTaO_3$ samples at 1 kHz [6]. Note that the fitting value of the carrier emission threshold field $E_m \approx U_m / h = 1455$ kV/cm is of the same order as the thermodynamic coercive field value of perfect $LiTaO_3$. The relatively small Debye screening radius $R_d = 100$ μm could be explained by the presence of numerous lithium vacancies reported by Fujimoto *et al.*

[6] as well as by the carriers injection from the tip. But the question about the applicability of our "equilibrium" calculations remains open due to the small duration of the applied voltage pulses $\sim 10^{-4}$ s. Despite this warning, we obtained rather well quantitative agreement between our fitting and experimental points.

The optimization procedure based on (8)-(10) gives that it is possible to record stable domains with $d_{min} \approx 8.5$ nm at $U_{cr} \approx 4.4$ V in the films with the thickness $h_{opt} \approx (20...30)$ nm. Thus, information recording with the density 338 Gbit/cm^2 is accessible in the thin $LiTaO_3$ films.

4. Conclusion

The obtained results will help researchers to achieve the reliable understanding of physical process taking place during the micro- and nanoscale polarization reversal in the ferroelectric-semiconducting media, as well as to determine the necessary experimental conditions in order to record stable nanodomains with optimum lateral sizes and configuration in order to increase recording density and create different profiled microstructures. Namely:

• The thermodynamical theory of nanodomain tailoring in ferroelectrics-semiconductors has been evolved allowing for semiconducting properties, screening and size effects. The contribution of these effects leads to the significantly new description of the physical processes taking place under the nanoscale polarization reversal, in particular, they determine equilibrium nanodomain sizes.

• It has been demonstrated that the domain appearance is similar to the well-known first order phase transition: the domain appears with non-zero minimum radius at definite critical voltage applied to the AFM tip.

The lateral sizes of nanodomains recorded at different voltages applied to the AFM tip were calculated in $BaTiO_3$, $LiNbO_3$ ferroelectric-semiconductors and $Pb(Zr,Ti)O_3$, $LiTaO_3$ thin films.

References

1. M.E. Lines, A.M. Glass, *Principles and applications of ferroelectrics and related phenomena.* Oxford University Press, Oxford, 1978.
2. V.M. Fridkin, *Ferroelectrics semiconductors.* Consultant Bureau, New-York and London, 1980.
3. A.N. Morozovska, E.A. Eliseev, V.V. Obukhovsky // *Ferroelectrics* **288,** p. 265-275 (2003).
4. A. Agronin, Y. Rosenwaks, and G. Rosenman // *Appl. Phys. Lett.* **85,** p. 452-454 (2004).
5. M. Molotskii, A. Agronin, P. Urenski, M. Shvebelman, Y. Rosenwaks and G. Rosenman // *Phys. Rev. Lett.* **90,** 107601-4 (2003).
6. K. Fujimoto, Y. Cho // *Appl. Phys. Lett.* **83,** p. 5265-5267 (2003).
7. P. Paruch, T. Tybell, J.-M. Triscone // *Appl. Phys. Lett.* **79**, p. 530-532 (2001).
8. C. Durkan, M. E. Welland, D.P. Chu, and P. Migliorato // *Phys. Rev. B* **60**, p. 16198–16204 (1999).
9. C.H. Ahn, K.M. Rabe, and J.-M. Triscone // *Science* **303**, p. 488-490 (2004).
10. T. Tybell, P. Paruch, T. Giamarchi, and J.-M. Triscone // *Phys. Rev. Lett.* **89**, 097601-4 (2002).
11. L.M. Eng, M. Bammerlin, Ch. Loppacher, M. Guggisberg, R. Bennewitz, R. Luthi, E. Meyer, Th. Huser, H. Heinzelmann and H.-J. Guntherodt // *Ferroelectrics* **222,** p. 153-159 (1999).
12. Y. Rosenwaks, D. Dahan, M. Molotskii, and G. Rosenman // *Appl. Phys. Lett.* **86**, 012909-3 (2005).
13. S.V. Kalinin, D.A. Bonnell, T. Alvarez, X. Lei, Z. Hu, R. Shao, and J.H. Ferris // *Adv. Mater.* **16**, p. 795-799 (2004).
14. J.F. Scott, *Ferroelectric memories.* Springer, Berlin and Heidelberg, 2000.
15. R. Landauer // *J. Appl. Phys.*, **28** p. 227-234 (1957).
16. M. Molotskii // *J.Appl. Phys.* **93** p. 6234-6237 (2003).
17. A.N. Morozovska, E.A. Eliseev // *Phys. status solidi* (*b*) **242**, p. R79-R81 (2005).
18. A.N. Morozovska, E.A. Eliseev // *E-print archive cond-mat* http://arxiv.org/cond-mat/0508045 (2005).
19. A.N. Morozovska, E.A. Eliseev // *E-print archive cond-mat* http://arxiv.org/cond-mat/0509450 (2005).
20. A.N. Morozovska, E.A. Eliseev // *J. Phys.: Condens. Matter*. **16**, p. 8937-8956 (2004).
21. A.N. Morozovska, E.A. Eliseev // *Phys. status solidi* (*b*) **242**, p. 947-961 (2005).
22. A.N. Morozovska, E.A. Eliseev // *Physica B*, **355,** p. 236-243 (2005).
23. X. Li, A. Mamchik, I.-W. Chen // *Appl. Phys. Lett.* **79**, p. 809-811 (2001).
24. B. Wang, and C.H. Woo // *J. Appl. Phys.* **94,** p. 4053-4059 (2003).
25. M. Molotskii // *J. Appl. Phys.* **97**, p. 014109-8 (2005).
26. S.V. Kalinin, E. Karapetian, M. Kachanov // *Phys. Rev. B* **70** 184101-24 (2004).
27. G.I. Rosenman, E.I. Boikova, Yu.L. Chepelev // *Phys. status solidi* (*a*) **69**, p. K1 73 − K1 77 (1982).
28. H. Kohlstedt, N.A. Pertsev, J. Rodrigues Contreras, R. Waser // *Phys. Rev. B* **72**, 125341-10 (2005).
29. M. Grossmann, O. Lonse, D. Bolten, U. Boettger, R. Waser // *J. Appl. Phys.* **92,** p. 2680-2696 (2002).
30. T. Tybell, C.H. Ahn, J.-M. Triscone // *Appl. Phys. Lett.* **75**, p. 856-858 (1999).
31. F. Felten, G.A.Schneider, J. Munoz Saldana, S.V. Kalinin // *J. Appl. Phys.* **96** p. 563-568 (2004).
32. J. Jang, G.C. Schatz, and M.A. Ratner // *J. Chem. Phys.* **120**, p. 1157-1160 (2004).
33. R.C. Miller, G. Weinreich // *Phys. Rev.* **117**, p. 1460-1466 (1960).
34. S. Poykko, D.J. Chadi // *Appl. Phys. Lett.* **75**, p. 2830-2832 (1999).
35. B. Meyer, D. Vanderbilt // *Phys. Rev. B* **65**, 104111-11 (2002).
36. J. Padilla, W. Zhong, D. Vanderbilt // *Phys. Rev. B* **53**, p. R5969-R5973 (1996).
37. C. Lichtensteiger, J.-M. Triscone, J. Junquera, P. Ghosez // *E-print archive cond-mat* http://arxiv.org/cond-mat/0404228 (2004).
38. D.D. Fong, G.B. S.K. Stephenson, Streiffer, J.A. Eastman, O. Auciello, P.H. Fuoss, C. Thompson // *Science* **304**, p. 1650-1653 (2004).
39. T.J. Yang, U. Mohideen // *Physics Letters A*, **250**, p. 205-210 (1998).
40. D.A. Scrymgeour, V. Gopalan, A. Itagi, A. Saxena, and P.J. Swart // *Phys. Rev. B* **71**, 184110-11 (2005).
41. M.D. Glinchuk, E.A. Eliseev, V.A. Stephanovich // *Physica B* **332**, p. 356-370 (2002).
42. M.D. Glinchuk, A.N. Morozovska // *J. Phys.: Condens. Matter*. **16,** p. 3517-3531 (2004).
43. L.E. Cross, Ferroelectric ceramics: Tailoring properties for specific application. In: *Ferroelectric ceramics* / Ed. N. Setter. Birkhauser Verlag, Basel, 1993.